



Published in final edited form as:

J Chem Inf Model. 2022 March 14; 62(5): 1282–1293. doi:10.1021/acs.jcim.1c01104.

Paired Simulations and Experimental Investigations into the Calcium-Dependent Conformation of Albumin

Dharmeshkumar Patel,

Institute for Modeling Collaboration and Innovation, University of Idaho, Moscow 83844 Idaho, United States; Laboratory of Biochemical Pharmacology, Department of Pediatrics, Emory University School of Medicine and Children's Healthcare of Atlanta, Atlanta 30322 Georgia, United States

Stephanie L. Haag,

Department of Chemical and Biological Engineering, University of Idaho, Moscow 83844 Idaho, United States

Jagdish Suresh Patel,

Institute for Modeling Collaboration and Innovation, University of Idaho, Moscow 83844 Idaho, United States; Department of Biological Sciences, University of Idaho, Moscow 83844 Idaho, United States

F. Marty Ytreberg,

Institute for Modeling Collaboration and Innovation, University of Idaho, Moscow 83844 Idaho, United States; Department of Physics, University of Idaho, Moscow 83844 Idaho, United States

Matthew T. Bernards

Department of Chemical and Biological Engineering, University of Idaho, Moscow 83844 Idaho, United States

Abstract

Serum albumin is the most abundant protein in blood plasma, and it is involved in multiple biological processes. Serum albumin has recently been adapted for improving biomaterial integration with bone tissue, and studies have shown the importance of this protein in bone repair and regeneration. However, the mechanism of action is not yet clear. In stark contrast, other studies have demonstrated that albumin blocks cell adhesion to surfaces, which is seen as a limitation to its bone healing role. These apparent contradictions suggest that the conformation

Corresponding Authors ytreberg@uidaho.edu, mbernards@uidaho.edu.

Author Contributions

The manuscript was written through contributions of all authors. All authors have given approval to the final version of the manuscript.

The authors declare no competing financial interest.

ASSOCIATED CONTENT

Supporting Information

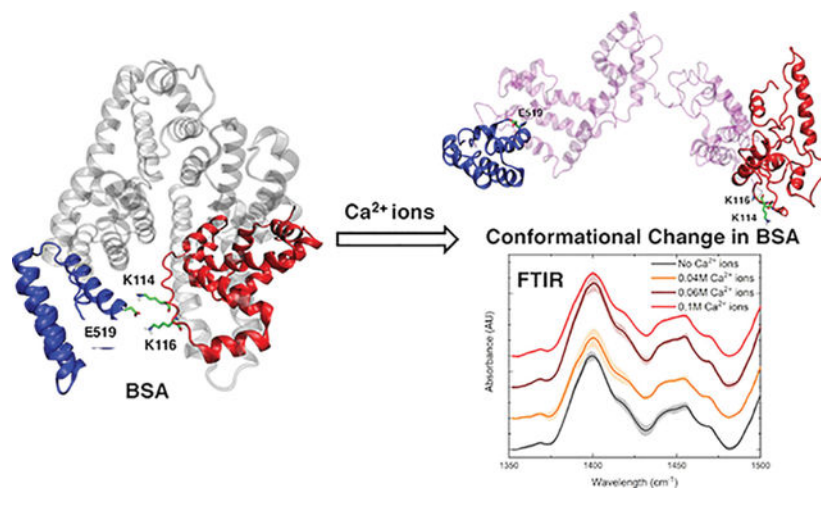
The Supporting Information is available free of charge at <https://pubs.acs.org/doi/10.1021/acs.jcim.1c01104>.

Calculation of ionic concentrations for CG simulations, distance between the oxygen atom of side chains or backbone residues of BSA and stably bound Ca^{2+} ions from the MD simulations of BSA with 30 Ca^{2+} ions and 11 Ca^{2+} ions, analysis of opening of BSA structure in MD trajectories with and without Ca^{2+} ions, and FTIR spectra for BSA and BSA exposed to multiple calcium concentrations, all after background subtraction (n = 9) (PDF)

Probable calcium-binding sites during CG simulations (XLSX)

of albumin facilitates its bioactivity, leading to enhanced bone repair. Serum albumin is known to play a major role in maintaining the calcium ion concentration in blood plasma. Due to the prevalence of calcium at bone repair and regeneration sites, it has been hypothesized that calcium binding to serum albumin triggers a conformational change, leading to bioactivity. In the current study, molecular modeling approaches including molecular docking, atomic molecular dynamics (MD) simulation, and coarse-grained MD simulation were used to test this hypothesis by investigating the conformational changes induced in bovine serum albumin by interaction with calcium ions. The computational results were qualitatively validated with experimental Fourier-transform infrared spectroscopy analysis. We find that free calcium ions in solution transiently bind with the three major loops in albumin, triggering a conformational change where N-terminal and C-terminal domains separate from each other in a partial unfolding process. The separation distance between these domains was found to correlate with the calcium ion concentration. The experimental data support the simulation results showing that albumin has enhanced conformational heterogeneity upon exposure to intermediate levels of calcium, without any significant secondary structure changes.

Graphical Abstract



INTRODUCTION

Serum albumin is the most abundant plasma protein in mammals and is key for controlling the levels of metals such as calcium in the blood. Furthermore, it is known that serum albumin enhances bone healing and regeneration and therefore has significant therapeutic potential.¹ For example, bone fracture sites have upregulated albumin production, and this upregulation results in an increase in bone calcium and DNA.² In addition, albumin has a role in osteoblast cell regulation including enhancing cell proliferation and stimulating collagen mRNA expression *in vitro*.^{3,4} Albumin has been used as a coating in tissue engineering applications to improve the biocompatibility by increasing cell adhesion, proliferation, and viability.^{5,6} It has also been shown to mediate adhesion to hydroxyapatite in a dose-dependent manner.⁷ Finally, the incorporation of albumin onto grafts implanted

at bone injury sites enhances healing of non-union defects, leading to the formation of mechanically stronger *de novo* bone.^{8–10}

Although the albumin literature has demonstrated its benefits when incorporated into tissue engineering constructs, it is not yet understood how albumin influences *in vivo* healing. Further complicating the picture is the fact that albumin has also been shown to prevent the adhesion of various cell types including bovine aortic endothelial cells and murine pre-osteoblast cells.^{7,11–14} Sivaraman *et al.* recently investigated the response of platelets to albumin-coated surfaces.^{15–17} They demonstrated that platelet adhesion to albumin-coated substrates is dependent on the conformation of albumin, and more specifically the relative levels of the secondary structure (α helix and β sheet content). Furthermore, platelet adhesion was correlated to the degree of adsorption-induced protein unfolding and loss of the secondary structure. This previously unrecognized cell adhesion bioactivity, coupled with the evidence that albumin increases healing in bone tissue, suggests that species present at bone regeneration sites such as ions may influence the conformation of albumin, leading to enhanced bioactivity. Therefore, we hypothesized that albumin exposure to calcium triggers a conformational change that in turn enhances the bioactivity of albumin. This hypothesis is supported by our previous work, demonstrating that albumin adsorbed to hydroxyapatite promotes significantly greater levels of cell adhesion than albumin adsorbed to control surfaces.⁷ This cellular response was also dependent on the level of albumin exposure, indicating that the enhanced adhesion was directly attributable to the presence of adsorbed albumin.

Despite the success of experimental techniques to determine the structural features of proteins,^{18–22} the experimental study of dynamic transitions between conformations remains extremely challenging. On the other hand, computational modeling and simulation offer the ability to study protein at the atomistic level, albeit at the expense of some accuracy.^{23,24} One such computational approach is molecular dynamics (MD) simulations that can provide atomistic details of the protein structure and dynamics and validate experimental observations.^{25,26} However, atomistic MD simulations can be very computationally expensive, especially if large-scale conformational changes are being studied. Such simulations are typically able to capture dynamics at the nanosecond to microsecond (ns to μ s) timescales.^{26,27} To increase these timescales, coarse-grained (CG) MD models can be used.^{26,28} In CG models, a mapping scheme is used to represent a group of atoms as beads, leading to a reduction in the degrees of freedom and hence longer simulation timescales. Recently, CG MD simulations have been widely used to investigate the large-scale conformational changes in a variety of biomolecules.²⁶ Efforts are still underway to continue to develop and improve CG force fields.^{29–32} Of particular interest, Pantano *et al.* developed a CG force field called SIRAH (<http://www.sirahff.com>) that has force field parameters for proteins,³³ nucleotides,³⁴ aqueous solvents,³⁵ and lipids.³⁶ In SIRAH, the CG topologies were developed by mapping the position of real atoms to CG beads.

In this work, molecular modeling was used to study the conformational changes in bovine serum albumin (BSA) at various concentrations of calcium ions, and these results were validated using Fourier-transform infrared (FTIR) spectroscopy. Computational molecular docking of calcium ions with BSA was first performed to identify possible calcium-binding

sites in BSA. These results were then used to perform atomistic MD simulations to verify the stability of bound calcium ions with BSA, as well as to identify initial conformational changes in BSA induced by calcium ion binding. It was observed that unbound calcium ions in the bulk solvent trigger conformational changes in BSA. To further investigate the large-scale conformational changes in BSA, CG simulations of BSA exposed to different concentrations of calcium ions were performed. The resulting conformational changes were evaluated through calculations of the CG backbone root-mean-square deviations (rmsd), residue-specific average rmsd of the C- α atom, solvent-accessible surface area (SASA), center of mass (COM) separation, and number of stably bound calcium ions. The CG simulations indicated that large-scale conformational changes occur in BSA with increasing calcium ion concentrations. In native BSA, the N-terminal and C-terminal domains are located adjacent to each other and upon increasing calcium concentration exposure, these domains become separated, moving away from each other in a calcium concentration-dependent manner. During this separation, there were no significant changes in the secondary structure of BSA. Finally, the results of the CG simulations were qualitatively validated using FTIR spectroscopy. The FTIR results support the conclusions from the MD simulations by showing enhanced conformational heterogeneity of BSA at intermediate calcium exposure concentrations with no significant secondary structural changes.

MATERIALS AND METHODS

System Preparation.

Molecular Docking.—To reproduce the binding modes of co-crystal calcium ions, molecular docking of calcium ions with BSA using different force fields was performed using AutoDock vina.³⁷ The 3D coordinates of BSA was retrieved from the Protein Data Bank (PDB; <https://www.rcsb.org>) for the docking study with calcium ions (PDB ID: 3V03).³⁸ In this PDB structure, there are three calcium ions co-crystallized with BSA. As a part of the protein preparation, water molecules and all of the ions were removed from the protein. Three docking procedures were performed to allow the validation of the docking protocols, using the partial charges for BSA and calcium ions from three different force fields: CHARMM,³⁹ PARSE,⁴⁰ and AMBER.⁴¹ The input files were prepared using the PDB2PQR server (<https://server.poissonboltzmann.org/pdb2pqr>) with neutral pH. The selection of the force fields used in the subsequent study was based on reproducing the three co-crystallized calcium ion-binding modes in the top docked poses. The number of binding poses in the docking simulations was increased until the three co-crystallized calcium ion-binding modes were reproduced. A grid box with size 104 Å × 88 Å × 78 Å with coordinates (x, y, z) of 47.59, 10.85, 36.77 was used, in order to cover the whole protein. For each configuration, the exhaustiveness value 100 was selected to obtain the binding poses. The final binding poses were analyzed and visualized using VMD software.⁴²

Atomistic MDs Simulations.—The calcium ion-binding poses obtained from molecular docking studies were selected for atomistic MD simulations to check the stability of the binding sites and their impact on the conformation of albumin. Three atomistic MD simulations of albumin with bound calcium ions were performed: (i) BSA with the top 30 unique binding poses from docking to screen for stability; (ii) BSA with stably bound

calcium ions obtained from simulation trajectories (i); and (iii) BSA with no calcium ions. The top 30 binding modes of calcium obtained using docking were selected and combined into a single structure file of BSA and used as the input for the atomistic MD simulations. BSA complexed with 30 calcium ions was solvated with a dodecahedron box of full atom TIP3P water molecules and ionized with Cl^- and Na^+ ions at a concentration of 0.150 M, in order to mimic physiological pH. The thickness of the water layer from the protein surface to the edge of the box was initially set to 1.5 nm. These conditions mimic the environment of healing bone, which has localized calcium levels as high as 40 mM^{43} in addition to the typically present ions. These conditions also mimic the prior experimental system that demonstrated enhanced albumin bioactivity when it is adsorbed to calcium releasing hydroxyapatite, which was completed in a 0.150 M buffer solution.⁷ The MD simulation was performed using GROMACS-2018.3⁴⁴ with the Amber99SB*ILDN⁴⁵ force field. Initially, the system was energy minimized, and then, equilibration MD simulations were performed with periodic boundary conditions. The temperature was equilibrated using an *NVT* ensemble for 1 ns followed by an *NPT* ensemble for 1 ns to equilibrate the pressure. Finally, the production MD simulations were performed for 200 ns under *NPT* conditions. The temperature and pressure were kept constant at 300 K and 1 atm, respectively, using a Berendsen thermostat and barostat.⁴⁶ A 2 fs simulation time step was used, and a snapshot was saved every 10 ps. The same protocol was used for the simulations mentioned in (ii) and (iii).

CG MDs Simulations.—A number of CG MD simulations of BSA with different concentrations of calcium ions were performed, in order to analyze the putative calcium-binding sites and large-scale conformational changes in BSA. CG MD simulations of BSA were performed at 0.02, 0.04, 0.06, 0.08, 0.1, 0.25, and 0.5 M calcium ion concentrations. A CG simulation of BSA without calcium ions was also performed as a reference.

CG simulations were performed using the SIRAH force field³³ (<http://www.sirahff.com>) for all of the systems according to the protocol reported in a study by Darré *et al.*³⁵ The CG topologies in SIRAH were developed by mapping the position of real atoms to CG beads. The distinctive features of the molecule to be CG and foreknowledge of the physiochemical properties are considered in the CG mapping. In CG topologies, polar or aromatic moieties are represented at a higher level of detail, while hydrophobic or bulky functional groups are described at a coarser level.^{33,35} In SIRAH, the use of partial charges on each bead maintains the properties to form hydrogen bond-like interactions and stabilize the secondary structure of the proteins without any constraints.³³ Hence, simple mapping procedures like the “four heavy atoms to one CG bead” rule used by the popular Martini force field⁴⁷ may be difficult to maintain important interactions in the protein structure.

Prior to mapping to the SIRAH CG model, protonation states of the 3D structure of BSA were generated using the PDB2PQR server⁴⁸ with the assumption of neutral pH and AMBER⁴¹ naming scheme as an output. Following the mapping to the CG model, the protein structure of BSA was placed in an octahedral box of SIRAH WT4 water molecules, and 2 nm of water thickness was selected. Then, the system was neutralized with Na^+ and Cl^- ions with a concentration of 0.150 M. Ca^{2+} and Cl^- were then added to each system of the albumin–water box to achieve the required calcium concentration for the simulations

(Supporting Information S1). Calcium at the CG level featured a point-charge of +2, a mass of 50 a.u., and differential van der Waals interactions.⁴⁹ Each system was minimized using the steepest descent for 10,000 steps, followed by 200 ns of equilibration simulation with step-by-step release of harmonically restrained backbone CG atoms of the protein. During the equilibration, the temperature of the systems was set to 300 K using the V-rescale thermostat,⁵⁰ and the pressure was set to 1 atm using the Parrinello–Rahman barostat⁵¹ with isotropic pressure coupling. The production CG simulations were performed for 20 μ s, with a time step of 20 fs. All of the CG simulations were repeated thrice. Electrostatic interactions are calculated using particle mesh Ewald⁵² with a direct cut off of 1.2 nm. A grid spacing of 0.2 nm was used for van der Waals interactions.

All of the CG simulations were carried out using GROMACS-2018.3.⁴⁴ The coordinate mapping and analysis were performed with SIRAH tools.⁵³ Rmsd was calculated for all of the C α , N, and O beads. The interactions between calcium and negatively charged protein beads were defined if calcium ions were within 3.5 Å of negatively charged protein beads. The visualization of CG trajectories was performed using the sirah_vmdtk.tcl plugin in VMD.^{42,53} The protein SASA values were calculated with the GROMACS utility gmx sasa, by setting a probe radius of 0.21 nm (*i.e.*, the radius of a WT4 bead). Radius of gyration (R_g) of the CG backbone atoms of BSA as a function of simulation time at different calcium concentrations and analysis of the separation distance between the COM of the two interacting domains, N-terminal domain-residue 3–150 and C-terminal domain-residue 502–583, were performed using written scripts based on the scripts provided in the VMD script library.

FTIR Spectroscopy Structural Analysis.—BSA (96%) was purchased from Sigma-Aldrich, and calcium chloride dihydrate was purchased from Fisher Scientific. Calcium chloride was dissolved into ultra-pure water (18.2 M Ω cm) to obtain concentrations of 0.02, 0.04, 0.06, 0.08, 0.1, 0.5, and 1.0 M. BSA solutions (100 mg/mL) were then prepared with ultra-pure water or one of the calcium chloride solutions. Ultra-pure water was used to isolate the impacts of calcium ions on the structure of albumin. A heat-denatured (HD) BSA solution in ultra-pure water was also prepared by heating the solution in an oven at 60 °C for 1 h. All samples were made 24 h prior to analysis with FTIR spectroscopy.

Spectra were collected using a Nicolet 6700 spectrometer with a circle attenuated total reflectance (ATR) cell. The spectra were recorded in triplicate between 4000 and 900 cm^{-1} by collecting and averaging 32 scans of each spectrum with a resolution of 4 cm^{-1} . Backgrounds of either water or one of the calcium solutions were collected before each BSA sample and then subtracted from the BSA solution spectra after data collection. Each condition was evaluated a minimum of three independent times, with a fresh sample being made each time. Data analysis was completed using OriginPro 2018.

RESULTS

The purpose of this study is to investigate the impacts of calcium concentration on the conformation and dynamics of albumin, in order to probe the hypothesis that calcium ion exposure triggers a more bioactive conformation of albumin that enhances bone repair. Our

strategy was to first perform molecular docking of calcium ions with BSA to predict the calcium-binding sites, followed by atomistic MD simulations of BSA with bound calcium ions, as predicted through molecular docking. The results of the atomistic simulations were expanded through CG simulations of BSA at additional concentrations of calcium ions, ranging from 0.02 to 0.5 M to probe for large-scale conformational changes. The CG simulations were analyzed for conformational change by calculating the rmsd of CG atoms and the residue-specific average rmsd of the C- α backbone atom of BSA. CG simulation results for BSA without calcium ion exposure were used as the reference, in order to extract the role of calcium on the conformational changes seen in the simulations. Finally, the results of the simulation studies were qualitatively validated using FTIR.

Prediction and Effect of Ca²⁺-Binding Sites on BSA.

In order to select the appropriate force field for completing calcium ion docking, top docked poses of calcium ions were evaluated using AMBER, CHARMM, and PARSE force field packages. The partial charges generated with the AMBER force field reproduced the original three calcium-binding modes identified in the crystal structure as part of the top 30 binding locations. In contrast, the partial charges generated by the CHARMM and PARSE force fields only reproduced two of the three calcium-binding modes identified in the crystal structure within the top 30 binding positions. Thus, the molecular docking results generated with the AMBER force field package were used for further studies.

The top 30 binding locations of calcium ions with BSA were used in atomistic MD simulations to study the stability of each of the binding sites and to analyze their impact on the conformation of albumin. Stable binding sites were defined as calcium ions that remained within 3.5 Å of their original binding location after 200 ns of simulation. Out of the 30 original calcium ions bound with BSA, 11 were found to be stable (Table 1, Figures 1C and S2).

Following 200 ns of simulation, conformational changes in BSA were evaluated by calculating the rmsd of the backbone atoms over the simulation time. Figure 1A shows the resulting rmsd plots of the backbone atoms of BSA, and the results demonstrate a comparatively larger rmsd when BSA is in the presence of 30 calcium ions relative to the rmsd without calcium ions. To further evaluate the impact of the stable calcium ions, an atomistic MD simulation of BSA with only the 11 stable, bound calcium ions was performed. Following 200 ns of simulation, 10 of the calcium ions remained stably bound, with the calcium ion leaving from binding site-9 (Figure S3 and Table 1). Of the 10 remaining ions, three calcium ions were bound in the locations found experimentally through X-ray crystal structure analysis, which were included in the original pdb structure; thus, seven new stable calcium-binding sites were predicted. In the MD simulations with only 11 calcium ions, the resulting rmsd of the BSA backbone atoms remained similar to the rmsd of BSA without calcium ions, especially when compared to the results with 30 calcium ions (Figure 1A). To further identify the regions in BSA with higher rmsd values, the residue-specific average rmsd of the C- α atoms were calculated for all three MD simulations of BSA (Figure 1B). The amino acid regions with the largest C- α variations were amino acid residue numbers 106–118, 292–314, and 490–516. These three regions correspond to

the three major loop regions of albumin, and they are highlighted in Figure 1C. It is also noted that in the residue-specific average rmsd results for BSA in the presence of 11 calcium ions, the greatest variation relative to the control simulation was seen for amino acid residue numbers 292–314, which correspond to the central loop region.

Calcium Concentration-Dependent Conformational Changes in BSA.

The large-scale conformational changes in BSA were investigated using CG simulations of BSA exposed to different concentrations of calcium ions. Initially, CG simulations of BSA were performed at 0.1, 0.25, and 0.5 M calcium concentrations to identify the occurrence of significant conformational changes. Figure 2A shows the resulting rmsd plots for the CG backbone atoms of BSA under these three exposure conditions. The results show that the rmsd drastically increases for BSA exposed to 0.1 M calcium, relative to the rmsd results for the other three conditions (0, 0.25, and 0.5 M). In contrast, the rmsd results for the CG backbone atoms of BSA exposed to 0.25 and 0.5 M calcium fluctuate very closely around the rmsd results for BSA without calcium. The residue-specific average rmsd of the CG C- α backbone atoms of BSA for all four scenarios, as shown in Figure 2B, show similar results to those seen in the atomistic MD simulations. The regions with the highest residue-specific average rmsd are again located in the amino acid residues that form the three major loops of BSA (Figure 1C).

To better understand the higher rmsd results for the CG simulation of BSA with 0.1 M calcium, four additional lower calcium ion concentrations (0.02, 0.04, 0.06, and 0.08 M) were investigated with CG simulations. All CG simulations, including the CG simulations of bovine albumin with 0.1 M calcium, were repeated thrice, and the results in Figure 3 show the overall average values of the rmsd of the CG backbone atoms as a function of simulation time. These results clearly show that the rmsd of the backbone atoms of BSA increased with increasing calcium concentration from 0 to 0.1 M.

The trajectories of the CG simulations were back mapped to the pseudo-atomistic form of BSA, and the overall structural changes were analyzed through visualization. As BSA is exposed to increasing levels of calcium, the overall structure opens up from the central loop region (residue number 292–314), and the salt bridges between K114 and E519 and K116 and E519 are broken (Figure 4A). A visual representation for this conformational change is shown in Figure 4B where the N-terminal domain and C-terminal domain are separated from each other. Figure 4C provides an overlay of the final BSA structure after CG simulations with 0.1 M calcium on the original crystal structure. To quantify the structural changes in BSA at different calcium concentrations, the Rg of the CG backbone atoms of BSA was analyzed as a function of simulation time for different concentrations (Figures 5A and S4A). The results show the average value of Rg increases at intermediate calcium concentrations, suggesting that the calcium is driving a conformational change in BSA. The opening of the protein structure also leads to changes in the relative distribution of exposed hydrophilic and hydrophobic surfaces of the protein. To determine the impact of calcium and the subsequent structural change on the level of exposed hydrophilic and hydrophobic surfaces, the SASA of BSA was calculated for the different CG simulations. The resulting histogram analysis of the SASA for each CG simulation is shown in Figure

5B and Supporting Information S4B, where it can be seen that the range of SASA for BSA increases at intermediate calcium concentrations. To better understand the breaking of the salt bridges between K114 and E519 and opening of the structure, the CG distance between two important H-bonded residues, K114 and E519, were analyzed through MD trajectories and plotted as a histogram, as shown in Figures 5C and S4C. The histogram plot shows that the CG atom distance between K114 and E519 gradually increases at intermediate calcium concentrations. Once the salt bridges break down between the C-terminal and N-terminal domains, these domains move further apart. To better understand and quantify this separation, we measured the distance between the COM of these domains (Figures 5D and S4D). The results are plotted as a histogram and show that the distance between the domains increases, again at intermediate calcium concentrations. These results are consistent with the increasing CG distance between two important H-bonded residues (Figure 5D), the SASA values (Figure 5B), and the simulation snapshot (Figure 4) that illustrates how the structure of BSA opens upon exposure to solvents with increasing calcium concentrations up to 0.1 M.

Finally, the number of calcium ions interacting with BSA was calculated to determine the free and bound calcium ions present during CG simulations at different calcium concentrations (Figure 6). While no significant structural changes were seen, this analysis included the CG simulation results for BSA exposed to 0.25 and 0.5 M calcium as well. Figure 6 shows that the number of calcium ions binding to BSA increases with increasing calcium concentrations, with a logarithmic-type dependency.

Experimental Validation of Simulation Results.

The CG simulation results indicate enhanced flexibility of BSA upon exposure to calcium concentrations up to 0.1 M, with enhanced stability at higher calcium concentration levels (0.25 and 0.5 M). Previous experimental studies have also shown that BSA can undergo numerous degrees of conformational changes, ranging from unfolding upon surface adsorption^{16,17} to being irreversibly denatured upon exposure to heat.⁵⁴ FTIR is one way of investigating these structural changes as it identifies molecular movement of key functional groups. Circle-ATR FTIR was chosen in this study to investigate the conformational changes in BSA in the presence of calcium in solution, to qualitatively support the simulation results.

It was previously shown that BSA undergoes significant heat-induced structural changes upon exposure to temperatures $60\text{ }^{\circ}\text{C}$,⁵⁴ so FTIR spectra for native and HD BSA were first collected as control spectra. Figure 7A shows representative spectra for both native BSA in water and HD BSA in water. The shape and magnitude of the amide I ($\sim 1545\text{ cm}^{-1}$) and amide II ($\sim 1650\text{ cm}^{-1}$) peaks dramatically change when BSA is denatured, confirming that the two amide peaks are strong indicators of BSA secondary structure. The amide I peak represents multiple C=O stretching vibrations, including carbonyl groups accepting no hydrogen bonds (1695 cm^{-1}), one hydrogen bond (1665 cm^{-1}), and two hydrogen bonds (1630 cm^{-1}), and antisymmetric stretching of COO⁻ side groups (1585 cm^{-1}).^{55,56} The amide II peak represents N-H bending for stronger hydrogen-bonded N-H groups (1550 cm^{-1}), weaker hydrogen-bonded N-H groups (1520 cm^{-1}), and free N-H groups (1500 cm^{-1}).^{55,56} Following the establishment of the experimental controls, FTIR spectra for

BSA in the presence of calcium (0.02, 0.04, 0.06, 0.08, 0.1, and 0.5 M) were collected and compared to that obtained for native BSA (Figures 7B and S5). Regardless of the calcium exposure level, no significant changes in the shape of the BSA amide peaks at 1545 and 1650 cm^{-1} are observed, unlike the drastic change seen following heat denaturing (Figure 7A). At the same time, there are changes to the intensity of the peaks, especially upon exposure to 0.06 M calcium. The lack of change to the overall peak shape suggests that exposure to calcium ions does not induce significant secondary structural changes to BSA, which supports the simulation results discussed above. As a result of this general agreement, a deconvolution of the amide I and II peaks was not undertaken as part of this investigation.

In evaluating the FTIR spectra (Figures 7 and S5), it is evident that there is increased variability in replicate FTIR spectra around 1400 and 1450 cm^{-1} for some of the calcium exposure concentrations. These FTIR peaks correspond to carboxylic acid O–H bending and α -methyl group C–H bending, respectively. Figure 7B provides a magnified look at the FTIR spectra for all of the replicate experimental measurements from 1350 to 1500 cm^{-1} (n = 9). The results clearly demonstrate there is significantly more sample to sample variation, as indicated by the standard deviation shading, when the BSA is exposed to 0.04 and 0.06 M calcium. Furthermore, when BSA is exposed to 0.06 M calcium, the intensity and the width of the peaks at 1400 and 1450 cm^{-1} increase relative to those for BSA in the absence of calcium. While each FTIR spectra represents an ensemble average of multiple BSA signals, these changes suggest that these exposure conditions lead to enhanced BSA conformational heterogeneity, especially upon exposure to 0.06 M calcium.

This is in qualitative agreement with the analysis of rmsd (Figure 3), R_g (Figure 5A), SASA (Figure 5B), critical salt bridge stability (Figure 5C), and COM of interacting domains (Figure 5D). At higher calcium concentrations (0.5 M), we see highly reproducible FTIR spectra, indicating increased structural stability that closely resemble the results for the native BSA (Figure 7C). The results for 0.5 M are in good agreement with the rmsd and MD trajectory analysis, as shown in Figures 2 and 5, respectively. Table 2 shows the computational prediction of conformational change at different calcium concentrations in comparison with experimental findings. The computational prediction was carried out using average rmsd, median SASA values, and average COM of interacting domains from the analysis of MD trajectories.

DISCUSSION

The objective of the present study is to investigate the influence of calcium on the conformation and secondary structure of albumin, to gain insights into the hypothesis that calcium triggers a bioactive conformational change to albumin. The starting point for this work was the crystal structure of BSA, which includes three calcium ions. This structure was used for calcium ion molecular docking simulations, leading to the identification of 19 loose docking sites and 11 stable, bound docking sites (including the original three from the crystal structure). Subsequent atomistic MD simulations revealed that BSA in the presence of 30 total calcium ions had a greater rmsd for the backbone atoms compared to both BSA in the presence of only 11 bound calcium ions and the native structure without calcium. These results suggest that conformational change, as indicated by the higher rmsd,

of BSA in the presence of 30 calcium ions is due to the bulk, free calcium ions rather than the stably bound calcium ions. To better identify the regions of BSA which undergo the most significant conformational change, the residue specific *C- α* rmsds were calculated for each of the three atomistic MD simulations. The most significant deviations in the *C- α* rmsd for BSA in the presence of 30 calcium ions were the three loop regions that connect the structured domains of BSA (residue numbers 106–118, 292–314, and 490–516). These results suggest that transient calcium interactions induce conformational changes to the loops without causing significant impact to the structured domains. Furthermore, even in the presence of the 11 stably bound calcium ions, the residue-specific *C- α* rmsd around the central loop (residue numbers 292–314) shows some deviation from the residue-specific *C- α* rmsd of BSA without calcium. This suggests that the conformationally induced bioactivity of albumin may be imparted by residues that become exposed upon changes near the central loop, again without any significant secondary structural changes.

The initial conformational studies were conducted with 200 ns of atomistic MD simulations. However, to better identify large-scale conformational changes in the protein structure, longer atomistic MD simulations would be required, and these are time consuming and not computationally cost-effective.^{26,27} In contrast, CG simulations are extremely efficient from a computational point of view as the number of atoms are reduced due to use of beads of atoms. Therefore, eight different calcium exposure concentrations were evaluated with 20 μ s CG simulations. The rmsd plots of the CG backbone atoms of BSA at different calcium concentrations show conformational changes in BSA for calcium concentrations 0.1 M but no significant changes in the rmsd for higher calcium concentrations. More specifically, the rmsd of the CG backbone atoms increases with increasing calcium concentration over a range from 0 to 0.1 M. To better understand the conformational changes, the trajectories of the CG simulations were visualized, and it is observed that the BSA structure opens around the central loop region. Furthermore, the structure opens more with increasing calcium concentrations, while no secondary structural changes are observed. This is in agreement with the atomistic MD simulations. In BSA, the N-terminus domain and the C-terminus domain are linked by hydrogen bonding between K114 (N-terminus domain) and E519 (C-terminus domain) and K116 (N-terminus domain) and E519 (C-terminus domain). During the opening of the structure, these bonds are broken, and the domains move away from each other. The regions adjacent to these H-bonds become exposed to the solvent (and binding interactions), so to quantify changes in the solvent-exposed region, the SASA was calculated for each of the CG simulations. Over the course of the CG simulation, the N-terminus and C-terminus domains of BSA fluctuate, especially considering the calcium-induced opening of the structure, so the average SASA values over the simulation time do not explain the dynamics of the structural changes. Rather, the histogram plots of SASA represent the frequency range over the course of the CG simulation, and they demonstrate that the solvent-exposed area of BSA is increased with increasing intermediate calcium concentration. The analysis of the R_g of the CG backbone atoms of BSA and the histogram analysis of the separation distance between the COM of the N-terminal and C-terminal domains further corroborate that the BSA structure is opening at intermediate calcium concentrations.

Finally, FTIR was used to qualitatively validate the atomistic MD and CG simulation results that both suggested that BSA undergoes conformational changes without any

CONCLUSIONS

In this study, we investigated the conformational changes induced in BSA by exposure to calcium ions *via* molecular modeling techniques including molecular docking, atomic MD simulations, and CG simulations. The modeling results demonstrated that interaction and binding of calcium ions with the three major loops trigger the conformational changes observed for BSA. The transient binding of calcium ions drives the conformational change of BSA. From the docking and MD simulations, seven additional stable calcium-binding sites were found that were not reported previously. As the calcium concentration increases, hydrogen bonding between the N-terminus domain and C-terminus domain is disrupted, leading to the separation of these domains. This separation leads to a subsequent increase in the R_g , SASA, and COM separation of BSA. However, at a certain calcium saturation level (~70% of the negatively charged amino acids), the BSA structure becomes less flexible. This indicates that regions of BSA not typically accessible are exposed upon this conformational change but only at intermediate calcium exposure levels. Furthermore, the modeling results confirmed that there is no significant loss of the secondary structure in BSA. The modeling results were qualitatively validated *via* FTIR spectroscopy, which suggest that BSA has enhanced conformational heterogeneity when exposed to 0.04 and 0.06 M calcium solutions. When taken in context with the existing literature demonstrating that albumin plays a role in enhanced bone healing and regeneration, the results of this study suggest there may be an as yet unidentified bioactive domain in albumin that becomes accessible upon the breakage of the hydrogen bond between the N-terminus and C-terminus domains. Therefore, this study provides a basis to further investigate and identify this possible bioactive domain in serum albumin through detailed experimental investigations into the conformational states of albumin upon exposure to calcium *via* more sensitive techniques.

Supplementary Material

Refer to Web version on PubMed Central for supplementary material.

Funding

This research was supported by the center for modeling complex interactions sponsored by the NIGMS under award no. P20 GM104420. Computer resources were provided in part by the Institute for Bioinformatics and Evolutionary Studies Computational Resources Core sponsored by the National Institutes of Health (grant no. P30 GM103324). This research also made use of the computational resources provided by the high-performance computing center at the Idaho National Laboratory, which is supported by the Office of Nuclear Energy of the U.S. Department of Energy (DOE) and the Nuclear Science User Facilities under contract no. DE-AC07-05ID14517. The funders had no role in study design, data collection, and analysis, decision to publish, or preparation of the manuscript.

DATA AND SOFTWARE AVAILABILITY

All of the PDB files were downloaded from the RCSB Protein Data Bank (<https://www.rcsb.org>). The following free pieces of software were used: Autodock Vina for molecular docking (<http://vina.scripps.edu/index.html>), PDB2PQR server to prepare files for docking (<https://server.poissonboltzmann.org/pdb2pqr>), and VMD for molecular visualization (<https://www.ks.uiuc.edu/Research/vmd/>). We used freely available force field parameters CHARMM, PARSE, and AMBER for docking the calcium ligand. All-atom and CG MD simulations were carried out with the freely available software

GROMACS (<http://www.gromacs.org/>). For all-atom MD simulations, freely available force field Amber99SB*ILDN, and for CG MD simulations, SIRAH force field (<http://www.sirahff.com>) were used, which is free. All the structures, MD trajectories, and experimental data mentioned in the article are available from the corresponding author upon reasonable request.

REFERENCES

- (1). Horváthy DB; Simon M; Schwarz CM; Masteling M; Vác G; Hornyák I; Lacza Z Serum albumin as a local therapeutic agent in cell therapy and tissue engineering. *Biofactors* 2017, 43, 315–330. [PubMed: 27859738]
- (2). Yamaguchi M; Igarashi A; Misawa H; Tsurusaki Y Enhancement of albumin expression in bone tissues with healing rat fractures. *J. Cell. Biochem.* 2003, 89, 356–363. [PubMed: 12704798]
- (3). Ishida K; Yamaguchi M Albumin regulates Runx2 and alpha1 (I) collagen mRNA expression in osteoblastic cells: comparison with insulin-like growth factor-I. *Int. J. Mol. Med.* 2005, 16, 689–694. [PubMed: 16142406]
- (4). Ishida K; Yamaguchi M Role of albumin in osteoblastic cells: enhancement of cell proliferation and suppression of alkaline phosphatase activity. *Int. J. Mol. Med.* 2004, 14, 1077–1081. [PubMed: 15547677]
- (5). Horváthy DB; Vác G; Cselenyák A; Weszl M; Kiss L; Lacza Z Albumin-coated bioactive suture for cell transplantation. *Surg. Innov.* 2013, 20, 249–255. [PubMed: 22717700]
- (6). Weszl M; Skaliczki G; Cselenyák A; Kiss L; Major T; Schandl K; Bognár E; Stadler G; Peterbauer A; Csöngé L; Lacza Z Freeze-dried human serum albumin improves the adherence and proliferation of mesenchymal stem cells on mineralized human bone allografts. *J. Orthop. Res.* 2012, 30, 489–496. [PubMed: 22371968]
- (7). Bernards MT; Qin C; Jiang S MC3T3-E1 cell adhesion to hydroxyapatite with adsorbed bone sialoprotein, bone osteopontin, and bovine serum albumin. *Colloids Surf., B* 2008, 64, 236–247.
- (8). Skaliczki G; Schandl K; Weszl M; Major T; Kovács M; Skaliczki J; Szendrői M; Dobó-Nagy C; Lacza Z Serum albumin enhances bone healing in a nonunion femoral defect model in rats: a computer tomography micromorphometry study. *Int. Orthop.* 2013, 37, 741–745. [PubMed: 23318937]
- (9). Schandl K; Horváthy DB; Doros A; Majzik E; Schwarz CM; Csöngé L; Abkarovits G; Bucsi L; Lacza Z Bone-Albumin filling decreases donor site morbidity and enhances bone formation after anterior cruciate ligament reconstruction with bone-patellar tendon-bone autografts. *Int. Orthop.* 2016, 40, 2097–2104. [PubMed: 27357530]
- (10). Horváthy DB; Vác G; Szabó T; Szigyártó IC; Toró I; Vámos B; Hornyák I; Renner K; Klára T; Szabó BT; Dobó-Nagy C; Doros A; Lacza Z Serum albumin coating of demineralized bone matrix results in stronger new bone formation. *J. Biomed. Mater. Res., Part B* 2016, 104, 126–132.
- (11). Liu L; Chen S; Giachelli CM; Ratner BD; Jiang S Controlling osteopontin orientation on surfaces to modulate endothelial cell adhesion. *J. Biomed. Mater. Res., Part A* 2005, 74, 23–31.
- (12). Kawashita M; Hayashi J; Kudo T.-a.; Kanetaka H; Li Z; Miyazaki T; Hashimoto M MC3T3-E1 and RAW264.7 cell response to hydroxyapatite and alpha-type alumina adsorbed with bovine serum albumin. *J. Biomed. Mater. Res., Part A* 2014, 102, 1880–1886.
- (13). Hindíé M; Degat M-C; Gaudière F; Gallet O; Van Tassel PR; Pauthe E Pre-osteoblasts on poly(L-lactic acid) and silicon oxide: Influence of fibronectin and albumin adsorption. *Acta Biomater.* 2011, 7, 387–394. [PubMed: 20692384]
- (14). Koblinski JE; Wu M; Demeler B; Jacob K; Kleinman HK Matrix cell adhesion activation by non-adhesion proteins. *J. Cell Sci.* 2005, 118, 2965–2974. [PubMed: 15976454]
- (15). Sivaraman B; Latour RA Time-dependent conformational changes in adsorbed albumin and its effect on platelet adhesion. *Langmuir* 2012, 28, 2745–2752. [PubMed: 22191731]

- (16). Sivaraman B; Latour RA Delineating the roles of the GPIIb/IIIa and GP-Ib-IX-V platelet receptors in mediating platelet adhesion to adsorbed fibrinogen and albumin. *Biomaterials* 2011, 32, 5365–5370. [PubMed: 21529934]
- (17). Sivaraman B; Latour RA The adherence of platelets to adsorbed albumin by receptor-mediated recognition of binding sites exposed by adsorption-induced unfolding. *Biomaterials* 2010, 31, 1036–1044. [PubMed: 19864017]
- (18). Levantino M; Yorke BA; Monteiro DC; Cammarata M; Pearson AR Using synchrotrons and XFELs for time-resolved X-ray crystallography and solution scattering experiments on biomolecules. *Curr. Opin. Struct. Biol.* 2015, 35, 41–48. [PubMed: 26342489]
- (19). Murata K; Wolf M Cryo-electron microscopy for structural analysis of dynamic biological macromolecules. *Biochim. Biophys. Acta, Gen. Subj* 2018, 1862, 324–334. [PubMed: 28756276]
- (20). Jiang Y; Kalodimos CG NMR Studies of Large Proteins. *J. Mol. Biol.* 2017, 429, 2667–2676. [PubMed: 28728982]
- (21). Okamoto K; Sako Y Recent advances in FRET for the study of protein interactions and dynamics. *Curr. Opin. Struct. Biol.* 2017, 46, 16–23. [PubMed: 29800904]
- (22). Lewis JH; Lu Z Integrating spatiotemporal features of a ligand-regulated, multi-state allosteric protein. *Nat. Struct. Mol. Biol.* 2019, 26, 816–822. [PubMed: 31488908]
- (23). Suresh A; Hung A Structural effects of divalent calcium cations on the alpha7 nicotinic acetylcholine receptor: A molecular dynamics simulation study. *Proteins* 2019, 87, 992–1005. [PubMed: 31228282]
- (24). Steel BC; McKenzie DR; Bilek MMM; Nosworthy NJ; dos Remedios CG Nanosecond responses of proteins to ultra-high temperature pulses. *Biophys. J.* 2006, 91, L66–L68. [PubMed: 16844754]
- (25). Patel D; Kuyucak S Computational study of aggregation mechanism in human lysozyme[D67H]. *PLoS One* 2017, 12, No. e0176886.
- (26). Dror RO; Dirks RM; Grossman JP; Xu H; Shaw DE Biomolecular simulation: a computational microscope for molecular biology. *Annu. Rev. Biophys.* 2012, 41, 429–452. [PubMed: 22577825]
- (27). Lane TJ; Shukla D; Beauchamp KA; Pande VS To milliseconds and beyond: challenges in the simulation of protein folding. *Curr. Opin. Struct. Biol.* 2013, 23, 58–65. [PubMed: 23237705]
- (28). Baaden M; Marrink SJ Coarse-grain modelling of protein-protein interactions. *Curr. Opin. Struct. Biol.* 2013, 23, 878–886. [PubMed: 24172141]
- (29). Chebaro Y; Pasquali S; Derreumaux P The coarse-grained OPEP force field for non-amyloid and amyloid proteins. *J. Phys. Chem. B* 2012, 116, 8741–8752. [PubMed: 22742737]
- (30). Krupa P; Halabis A; mudzi ska W; Oldziej S; Scheraga HA; Liwo A Maximum Likelihood Calibration of the UNRES Force Field for Simulation of Protein Structure and Dynamics. *J. Chem. Inf. Model.* 2017, 57, 2364–2377. [PubMed: 28809487]
- (31). de Jong DH; Singh G; Bennett WFD; Arnarez C; Wassenaar TA; Schäfer LV; Periole X; Tieleman DP; Marrink SJ Improved Parameters for the Martini Coarse-Grained Protein Force Field. *J. Chem. Theory Comput.* 2013, 9, 687–697. [PubMed: 26589065]
- (32). Han W; Schulten K Further Optimization of a Hybrid United-Atom and Coarse-Grained Force Field for Folding Simulations: Improved Backbone Hydration and Interactions between Charged Side Chains. *J. Chem. Theory Comput* 2012, 8, 4413–4424. [PubMed: 23204949]
- (33). Darré L; Machado MR; Brandner AF; González HC; Ferreira S; Pantano S SIRAH: A Structurally Unbiased Coarse-Grained Force Field for Proteins with Aqueous Solvation and Long-Range Electrostatics. *J. Chem. Theory Comput.* 2015, 11, 723–739. [PubMed: 26575407]
- (34). Dans PD; Zeida A; Machado MR; Pantano S A Coarse Grained Model for Atomic-Detailed DNA Simulations with Explicit Electrostatics. *J. Chem. Theory Comput.* 2010, 6, 1711–1725. [PubMed: 26615701]
- (35). Darré L; Machado MR; Dans PD; Herrera FE; Pantano S Another Coarse Grain Model for Aqueous Solvation: WAT FOUR? *J. Chem. Theory Comput* 2010, 6, 3793–3807.
- (36). Barrera EE; Frigini EN; Porasso RD; Pantano S Modeling DMPC lipid membranes with SIRAH force-field. *J. Mol. Model.* 2017, 23, 259. [PubMed: 28799119]

- (37). Trott O; Olson AJ AutoDock Vina: improving the speed and accuracy of docking with a new scoring function, efficient optimization, and multithreading. *J. Comput. Chem.* 2010, 31, 455–461. [PubMed: 19499576]
- (38). Majorek KA; Porebski PJ; Dayal A; Zimmerman MD; Jablonska K; Stewart AJ; Chruszcz M; Minor W Structural and immunologic characterization of bovine, horse, and rabbit serum albumins. *Mol. Immunol.* 2012, 52, 174–182. [PubMed: 22677715]
- (39). Huang J; MacKerell AD Jr. CHARMM36 all-atom additive protein force field: validation based on comparison to NMR data. *J. Comput. Chem.* 2013, 34, 2135–2145. [PubMed: 23832629]
- (40). Sitkoff D; Sharp KA; Honig B Accurate Calculation of Hydration Free Energies Using Macroscopic Solvent Models. *J. Phys. Chem.* 1994, 98, 1978–1988.
- (41). Hornak V; Abel R; Okur A; Strockbine B; Roitberg A; Simmerling C Comparison of multiple Amber force fields and development of improved protein backbone parameters. *Proteins* 2006, 65, 712–725. [PubMed: 16981200]
- (42). Humphrey W; Dalke A; Schulten K VMD: visual molecular dynamics. *J. Mol. Graphics* 1996, 14, 33–38.
- (43). Silver I; Murrills RJ; Etherington DJ Microelectrode studies on the acid microenvironment beneath adherent macrophages and osteoclasts. *Exp. Cell Res.* 1988, 175, 266–276. [PubMed: 3360056]
- (44). Van der Spoel D; Lindahl E; Hess B; Groenhof G; Mark AE; Berendsen HJC GROMACS: fast, flexible, and free. *J. Comput. Chem.* 2005, 26, 1701–1718. [PubMed: 16211538]
- (45). Maier JA; Martinez C; Kasavajhala K; Wickstrom L; Hauser KE; Simmerling C ff14SB: Improving the Accuracy of Protein Side Chain and Backbone Parameters from ff99SB. *J. Chem. Theory Comput* 2015, 11, 3696–3713. [PubMed: 26574453]
- (46). Berendsen HJC; Postma JPM; van Gunsteren WF; DiNola A; Haak JR Molecular dynamics with coupling to an external bath. *J. Chem. Phys.* 1984, 81, 3684–3690.
- (47). Marrink SJ; Risselada HJ; Yefimov S; Tieleman DP; de Vries AH The MARTINI Force Field: Coarse Grained Model for Biomolecular Simulations. *J. Phys. Chem. B* 2007, 111, 7812–7824. [PubMed: 17569554]
- (48). Dolinsky TJ; Nielsen JE; McCammon JA; Baker NA PDB2PQR: an automated pipeline for the setup of Poisson-Boltzmann electrostatics calculations. *Nucleic Acids Res.* 2004, 32, W665–W667. [PubMed: 15215472]
- (49). Cali T; Frizzarin M; Luoni L; Zonta F; Pantano S; Cruz C; Bonza MC; Bertipaglia I; Ruzzene M; De Michelis MI; Damiano N; Marin O; Zanni G; Zanotti G; Brini M; Lopreiato R; Carafoli E The ataxia related G1107D mutation of the plasma membrane Ca²⁺ ATPase isoform 3 affects its interplay with calmodulin and the autoinhibition process. *Biochim. Biophys. Acta, Mol. Basis Dis* 2017, 1863, 165–173. [PubMed: 27632770]
- (50). Bussi G; Donadio D; Parrinello M Canonical sampling through velocity rescaling. *J. Chem. Phys.* 2007, 126, 014101. [PubMed: 17212484]
- (51). Parrinello M; Rahman A Polymorphic transitions in single crystals: A new molecular dynamics method. *J. Appl. Phys.* 1981, 52, 7182–7190.
- (52). Essmann U; Perera L; Berkowitz ML; Darden T; Lee H; Pedersen LG A smooth particle mesh Ewald method. *J. Chem. Phys.* 1995, 103, 8577–8593.
- (53). Machado MR; Pantano S SIRAH tools: mapping, backmapping and visualization of coarse-grained models. *Bioinformatics* 2016, 32, 1568–1570. [PubMed: 26773132]
- (54). Shanmugam G; Polavarapu PL Vibrational circular dichroism spectra of protein films: thermal denaturation of bovine serum albumin. *Biophys. Chem.* 2004, 111, 73–77. [PubMed: 15450377]
- (55). Grdadolnik J; Maréchal Y Bovine serum albumin observed by infrared spectrometry. I. Methodology, structural investigation, and water uptake. *Biopolymers* 2001, 62, 40–53. [PubMed: 11135191]
- (56). Grdadolnik J; Maréchal Y Bovine serum albumin observed by infrared spectrometry. II. Hydration mechanisms and interaction configurations of embedded H₂O molecules. *Biopolymers* 2001, 62, 54–67. [PubMed: 11135192]
- (57). Praprotnik M; Janežič D; Mavri J Temperature Dependence of Water Vibrational Spectrum: A Molecular Dynamics Simulation Study. *J. Phys. Chem. A* 2004, 108, 11056–11062.

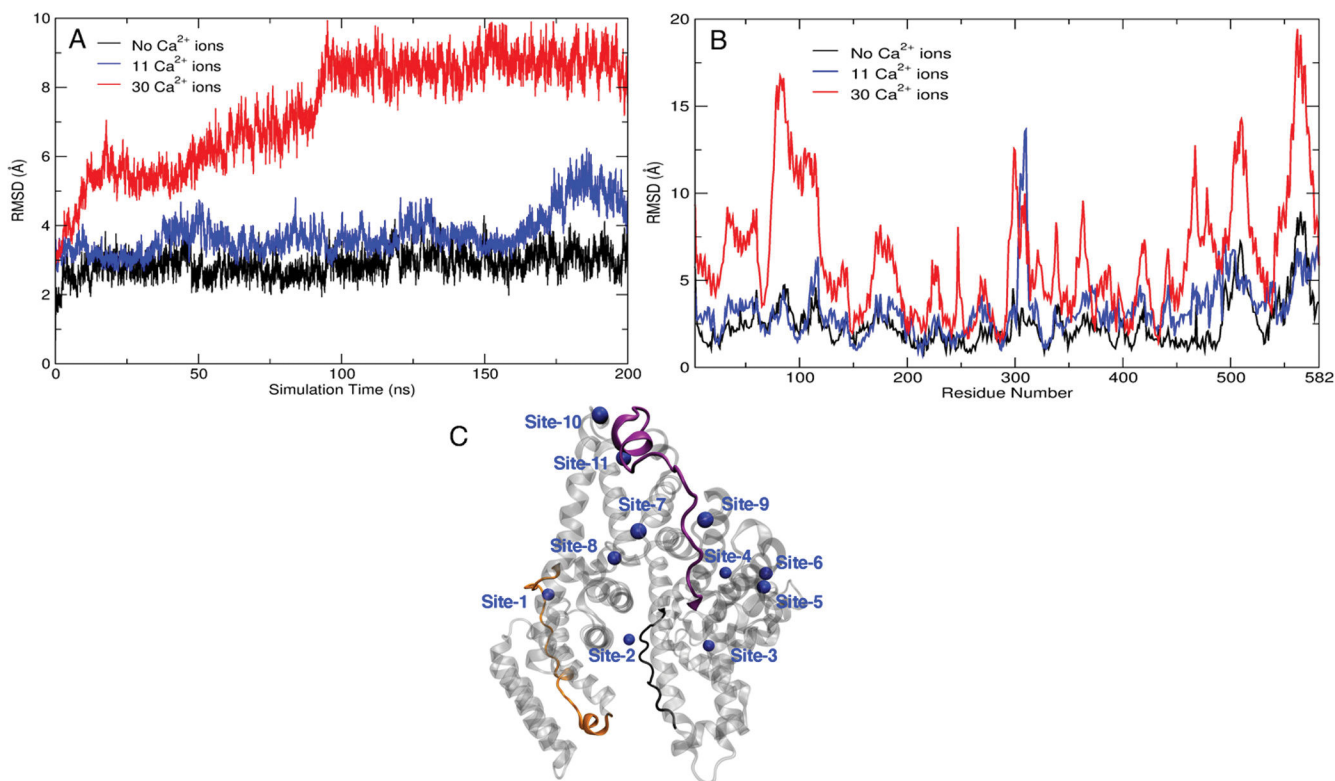


Figure 1. Analysis of the BSA conformation in the presence (30 or 11 calcium ions) and absence of calcium ions following atomistic MD simulations. (A) Rmsd of the backbone atoms of BSA as a function of MD simulation time. (B) Residue-specific average rmsd of the C- α atoms of BSA following 200 ns of MD simulation. (C) Binding locations for bound calcium ions (blue spheres) as identified from molecular docking and atomistic MD simulations. The three major loops of BSA corresponding to residue numbers 106–118 (black), 292–314 (violet), and 490–516 (orange) are involved in transient binding with calcium ions and are the primary source of conformational changes.

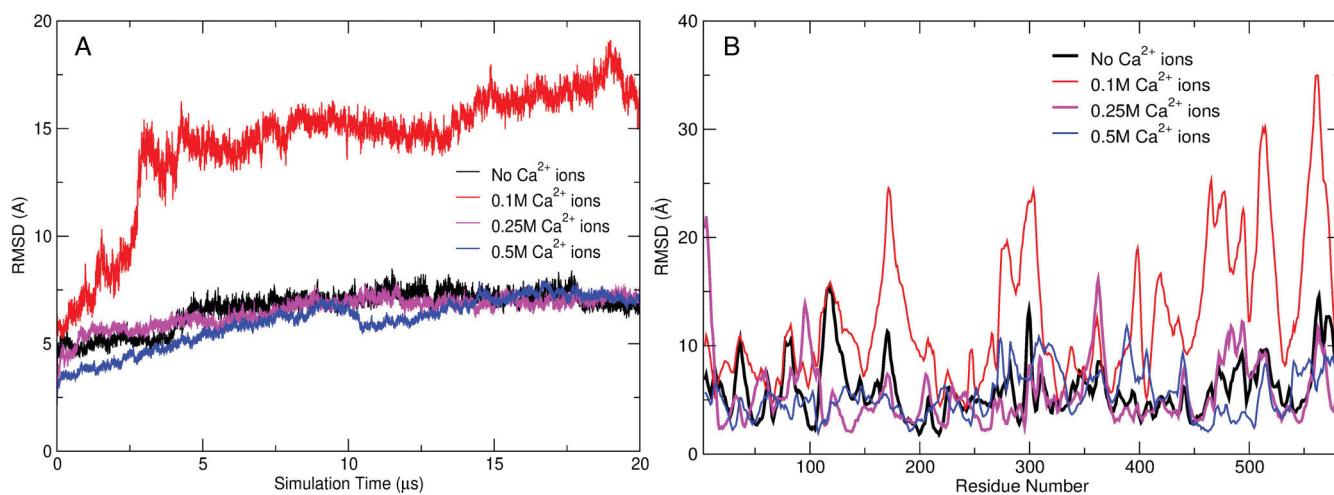


Figure 2. Analysis of BSA conformation in the presence (0.1, 0.25, or 0.5 M) and absence of calcium ions following CG simulations. (A) Rmsd of the CG backbone atoms for BSA as a function of CG simulation time. (B) Residue-specific average rmsd of the C- α atoms of BSA following 20 μ s of CG simulation.

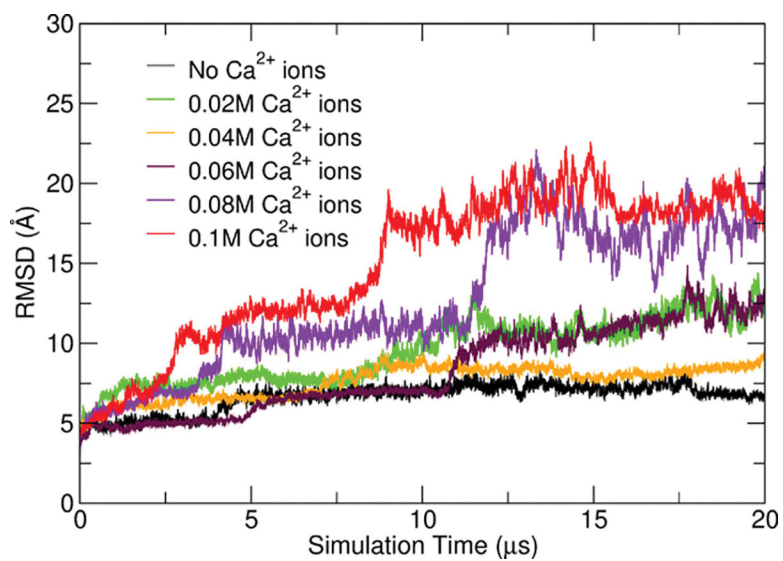


Figure 3. Rmsd analysis of the CG backbone atoms for BSA at different concentrations of Ca²⁺ ions as a function of CG simulation time.

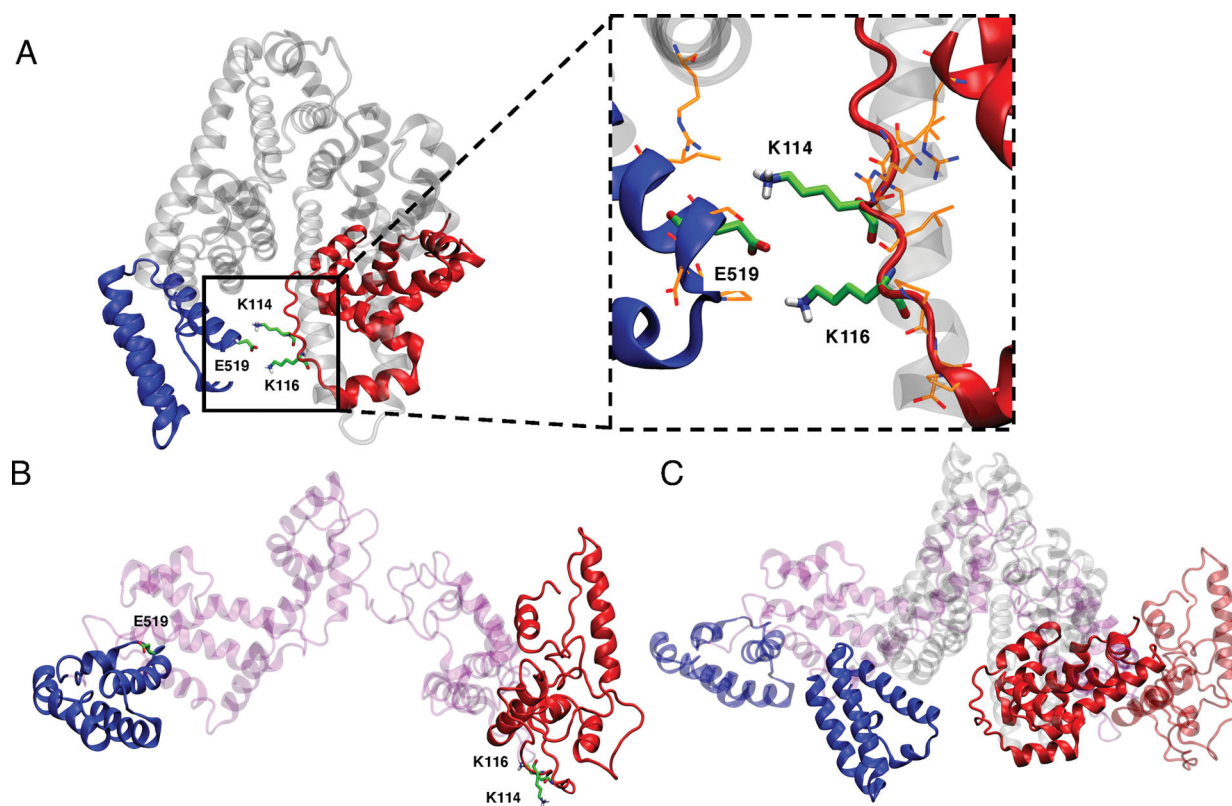


Figure 4.

A) 3D structure of BSA with hydrogen bonding between E519 from the C-terminus domain (blue colored) and K114 and K116 from the N-terminus domain (red colored). (B) Simulated albumin structure after exposure to 0.1 M calcium (magenta), with the C-terminus domain (blue colored) and N-terminus domain (red colored) separating from each other. (C) Simulated albumin structure after exposure to 0.1 M calcium (magenta) super-positioned with the original pdb crystal structure (gray). The C-terminus domain (blue colored) and N-terminus domain (red colored) are highlighted.

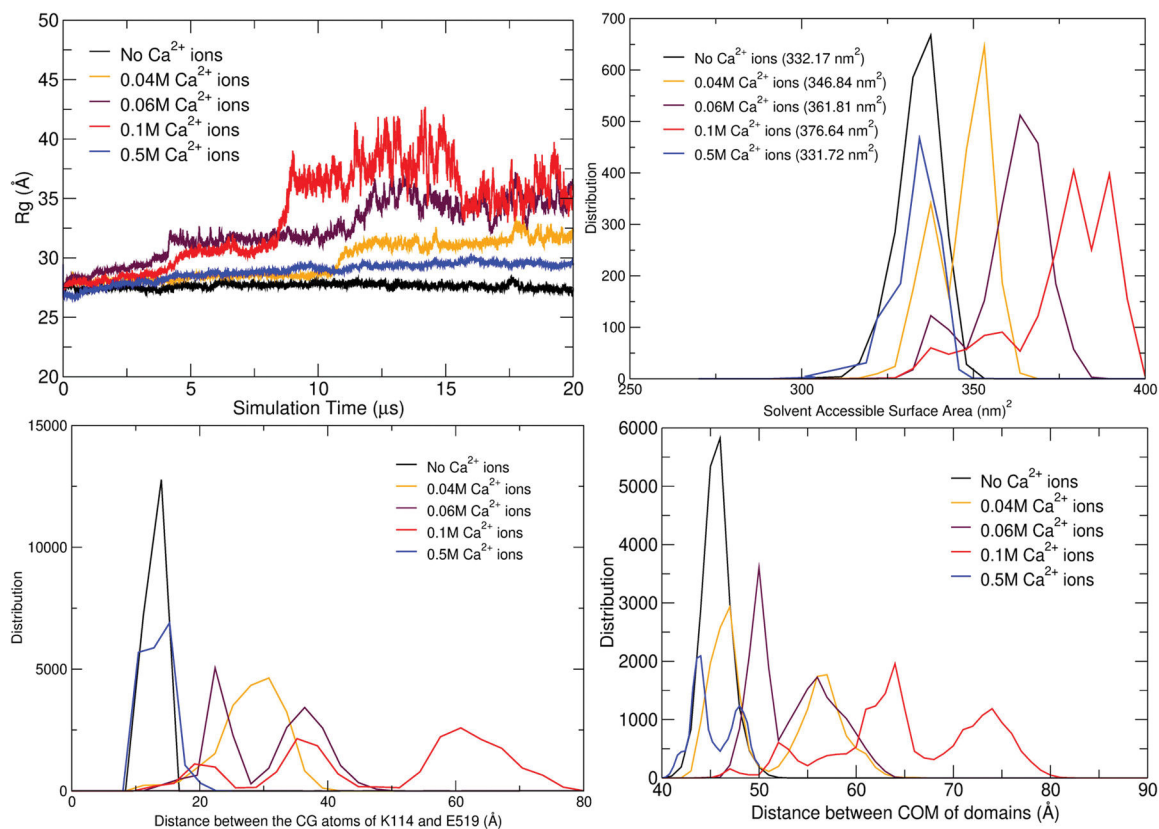


Figure 5.

Analysis of the opening of the BSA structure: (A) R_g of the CG backbone atoms of BSA as a function of simulation time at different calcium concentrations. (B) Histogram of the SASA of BSA from CG simulations for different concentrations of calcium ions. (C) Histogram of the distance between CG atoms of two important H-bonded residues, K114 and E519. (D) Histogram of the COM separation between the two interacting BSA domains.

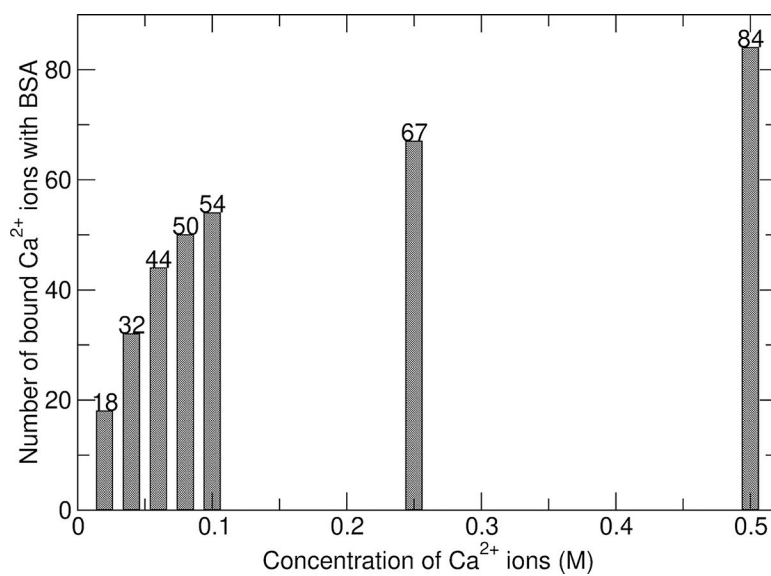


Figure 6. Number of Ca^{2+} ions binding to BSA following CG simulations with different calcium concentrations.

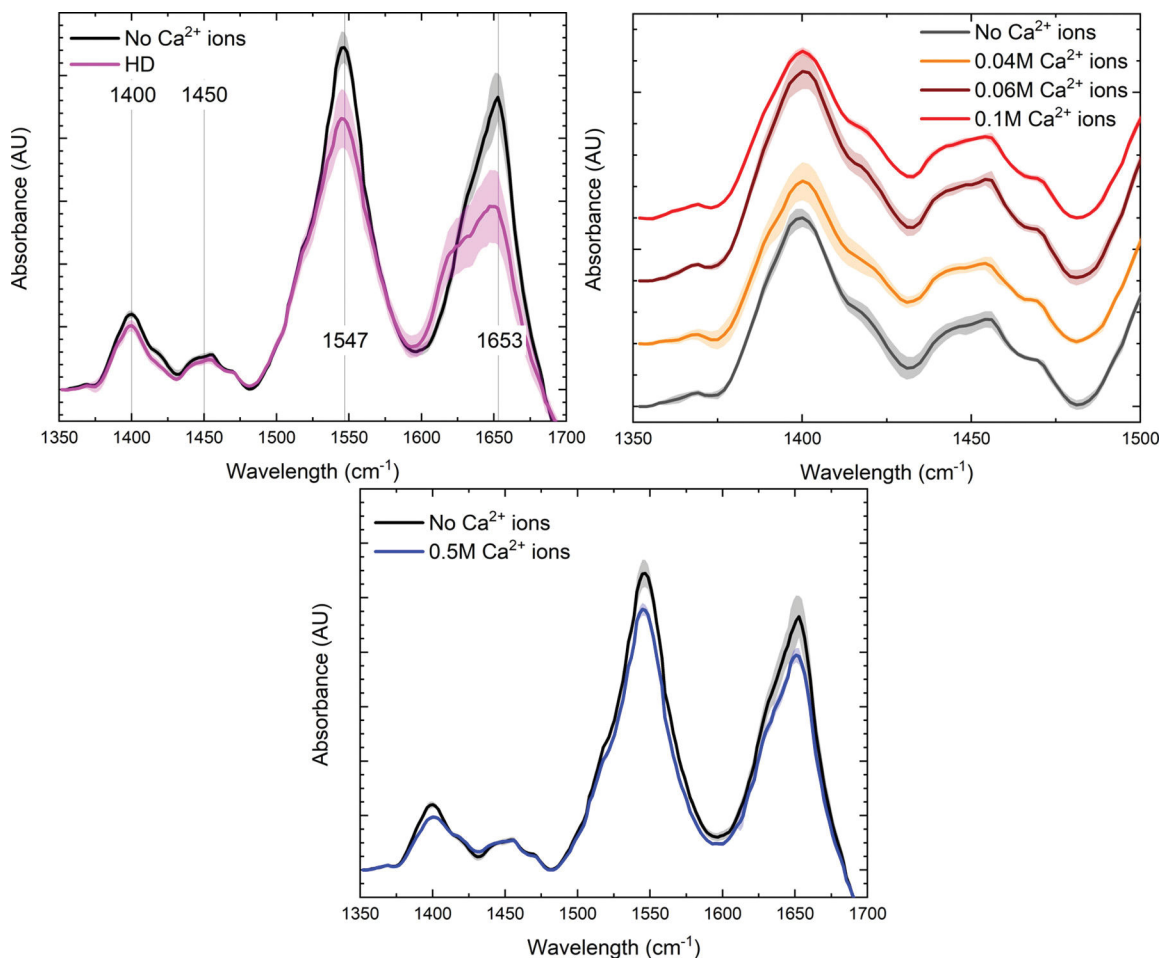


Figure 7. Average FTIR spectra for (A) BSA and HD BSA in solution, indicating significant loss of the secondary structure upon heat denaturation, (B) BSA and BSA exposed to multiple calcium concentrations, and (C) for BSA and BSA exposed to 0.5 M calcium, indicating the structural stability and similarity for these two experimental conditions. All of the FTIR spectra were subjected to background subtraction, and the standard deviation of replicate measurements is shown with color shading ($n = 9$).

Table 1.

Negatively Charged Side Chain or Backbone Amino Acids Responsible for the 11 Longer-term Stably Bound Ca^{2+} Ions, as Determined from Atomistic MD Simulations^a

binding site number	Ca-binding sites
1	R412, K413, T491, D493
2	S109, D111
3	L24, F27, S28
4	E243, D248, E251
5	D13, D254, D258
6	D13, D254, D258
7	Y333, S334, E339
8	S343, V481
9	A225, K224, F222
10	F308, Y352
11	E310, S370

^aThe three experimentally identified stable Ca^{2+} -binding sites previously determined are indicated in bold.

Table 2.

Comparisons of Computational Findings with the Experimental Results

Ca ²⁺ concentration (M)	average rmsd (Å)	median SASA (nm ²)	average distance between COM of the domains (Å)	conformational change in BSA (computational)	BSA heterogeneity (FTIR experiment)
no Ca ²⁺ ion	6.64	332.17	45.16	no	no
0.02	9.48	342.70	48.36	yes	no
0.04	7.59	346.84	50.69	yes	yes
0.06	8.23	361.81	53.03	yes	yes
0.08	12.62	363.15	59.98	yes	no
0.1	14.29	376.64	65.01	yes	no
0.25	6.52	330.28	46.23	no	no
0.5	6.03	331.72	45.55	no	no